Materials Science and Technology (MS&T) 2013
October 27-31, 2013, Montreal, Quebec, Canada
Copyright © 2013 MS&T'13®
Light Metals for Transportation

MESO-SCALE MODELLING ON RIDGING OR ROPING OF ALUMINIUM ALLOYS

Ling Qin[1]; Marc Seefeldt[1]; Paul Van Houtte[1];

[1]KU Leuven, Department of Metallurgy and Materials Engineering, Kasteelpark Arenberg 44 – box 2450, B-3001 Heverlee, Belgium

Keywords: moving window, AA6016 alloys, Roping, Lankford coefficient, EBSD, texture banding

Abstract

Aluminium alloys for automobile body panel application often show a specific type of band-shaped surface roughening upon stretching, called “ridging” or “roping”. Extensive research has indicated that the evolving surface roughness profiles are related to surface texture patterning. This work presents a “Moving window” method for detecting such texture patterning based on EBSD orientation maps. The measured EBSD map can be subdivided by the moving window, within which the orientation information is selected to represent the local texture. Then, the full constraint Taylor crystal plasticity model is used to simulate the Lankford coefficient (also called *r*-value) based on texture. By varying the size of the moving window in the transverse direction, the texture patterning in terms of the Lankford coefficient can be studied. Two samples with different roping tendency are studied in this work.

Introduction

The use of light-weight metals in a highly innovative automotive industry has increased significantly due to both economic and ecological reasons [1]. Special attention has been focused on heat-treatable Al-Mg-Si alloys of the AA6xxx series. These heat-treatable alloys achieve their final strength after the paint-bake cycle. Hence, a desired combination of good formability of the solution-treated state (T4 temper) with the increased service strength of the age-hardened state (T6 or T8) can be obtained for those AA6xxx alloys [2]. However, some AA6xxx alloys suffer from a phenomenon called ridging or roping.

Roping is a type of surface roughness, which is frequently observed after a tensile test in the transverse direction (TD) applied on aluminium sheets for car body application. Specifically, it is a series of ridges and valleys along the rolling direction. According to the literature, those ridges are approximately 5-50 mm in length, 10-30 μm in depth [3] and 1-2 mm apart in TD [4]. This drawback limits the use of aluminium alloys for the exterior car body panel application. Much effort has been focused on correlating roping with crystallographic texture by means of fully automated electron backscattered diffraction (EBSD) technique. Clustering of similarly orientated grains, i.e., texture banding, has been found by several research groups [2, 5-7]. Furthermore, EBSD orientation maps have been used as input to simulate roping with the help of crystal-plasticity models. However, the use of EBSD maps as an input for the roping model

naturally limits the simulation to the analysis of the behavior of two-dimensional sections through the sample, typically in the RD/TD rolling plane [8]. This work proposes a 'moving window' mechanical model to simulate the roping tendency based on EBSD orientation maps by using the Full Constraint Taylor model embedded in the MTM-FHM software system [9].

The Lankford coefficient is frequently referred to as the "*r*-value". It is defined as the ratio of the width to the thickness strain when the sample is subject to a uniaxial tensile test (UT). Thus, it can serve as a parameter to characterize resistance to strain thinning under loading.

Experimental

Two commercial AA6016 T4 sheets with different roping levels are studied in this work. The sample taken from the sheet, which is known to show severe roping after tensile plastic deformation in TD, is designated as roping susceptible. The other one was taken from the sheet yielding little roping after stretching in TD; it is designated as roping resistant. Both samples are prior to the final forming process with a thickness of about 1 mm.

Micro-texture measurements on the surface (rolling plane) of the two different samples were conducted by means of automated EBSD using a Dualbeam FEI Nova 600 Nanolab Scanning Electron Microscope (SEM). Prior to the EBSD measurement, both samples were mechanically polished to 0.25 μm followed by electro-polishing (30V, -30^{o}C) for 60s using an electrolytic solution consisting of 70% ethanol, 10% 2-butoxyethanol, 8% perchloric acid and 12% distilled water. About 60 μm of material in thickness was removed by polishing. In the EBSD measurement, the accelerating voltage of the Field Emission Gun (FEG) used was 15kV and the beam current was 8.9nA. The sample tilt angle was 70^{o} and binning was 8×8 when recording the Kikuchi patterns, which were indexed by the classic Hough transformation. Large-scale EBSD maps with a size of 7800 μm in TD and 2600μm in RD were obtained at a low magnification (80X) with a working distance of 15cm. The scanning step size of the EBSD measurement was 8 μm, leading to 318176 data points for each sample. The average grain size of both samples was about 30 μm calculated by the TSL OIM software using EBSD orientation maps.

The EBSD orientation maps for the roping susceptible and resistant samples are shown in Fig. 1 (a) and Fig. 1 (b) respectively. The normal direction (ND) inverse pole figure color coding strategy is illustrated by the unit triangle on top of the EBSD maps in Fig. 1. It can be seen in Fig. 1 (a) and (b) that the roping susceptible sample exhibits more ND//[101] orientated grains than the roping resistant. However, no clear distinction of texture components banding propensity can be observed based on such EBSD maps.

The Orientation Distribution Functions were calculated by the MTM-FHM software system [9] using the discrete EBSD orientation data. Fig. 1 (c) and (d) show the ODF's of the two samples with main texture components, namely, Cube, Goss, S, CG (i.e., RD-27^{o}-rotated Cube) and CH (i.e., ND-27^{o}-rotated Cube), marked out. Note that the same contour levels of the ODF intensity were used to facilitate comparison. The roping susceptible sample [Fig. 1 (c)] has a stronger texture with texture index of 3.138 than the roping resistant sample [Fig. 1 (d)] with texture index of 2.066. The Goss component can be observed in the roping susceptible sample but not in the roping resistant sample as shown in Fig. 1 (c) and (d).

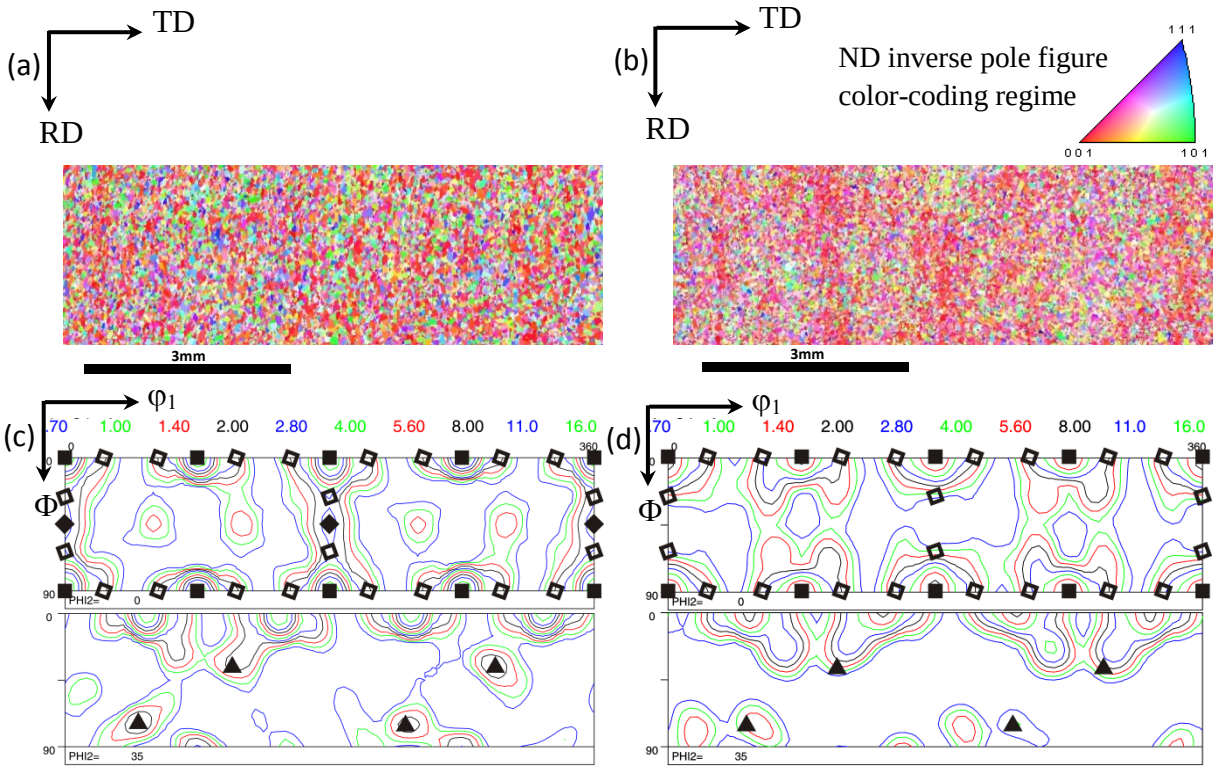

Fig. 1 Measured EBSD orientation maps for (a) the roping susceptible sample and (b) the roping resistant sample. φ_2=*0*^{o} and φ_2=*35*^{o} ODF sections calculated based on the discrete EBSD texture data for (a) the roping susceptible sample and (b) the roping resistant sample with Cube (■), Goss (◆), S (▲), CG (◘) and CH (◘) texture components identified.

Table I Volume fractions of the typical texture components in cold rolled and recrystallized AA6016-T4 aluminium alloys for the roping susceptible and resistant samples and simulated *r*-values for each texture component in three directions

Texture component	Index notation {hkl}<uvw>	Volume fraction (%)		Simulated *r*-value		
		Roping susceptible	Roping resistant	r_{RD}	r_{45}	r_{TD}
Cube	{001}<100>	17.2	12.2	1.00	0.00	1.00
Goss	{011}<100>	4.7	1.9	1.00	0.40	+∞
S	{123}<634>	17.2	16.2	0.67	5.80	0.49
CG	{021}<100>	13.7	8.9	1.00	0.14	6.89
CH	{001}<120>	12.5	14.3	0.15	0.36	0.15
5225-T Taylor	{4 4 11}<11 11 8>	8.0	10.1	0.30	3.26	0.05
Brass	{011}<211>	6.8	5.2	0.27	7.93	1.00
Copper	{112}<111>	7.6	8.3	1.00	5.99	0.11
H	{001}<110>	3.3	4.3	0.00	1.00	0.00
P	{011}<122>	5.7	7.7	8.26	1.06	0.31
Random texture				1.00	1.00	1.00

The volume fractions of typical texture components in cold rolled and recrystallized AA6016-T4 aluminium alloys were computed by using the MTM-FHM software system [9]. Table I shows the calculated volume fractions (in percentage) of texture components for the two samples. Among all the listed components, Cube, S, CG and CH are predominant in both samples. The volume fraction of Goss is relatively low among all the listed texture components in both samples. However, the roping susceptible sample contains more than 2 times of the Goss component than the roping resistant one. Moreover, the volume fraction of CG in the roping susceptible is larger than that in the roping resistant one. This is in agreement with ODF observation shown in Fig. 1 (c) and (d).

Based on the ODF's of both samples, *r*-value can be simulated by using the MTM-FHM software system [9]. The theoretical proof of *r*-value simulation is given in the appendix of Ref. [10]. Table I also shows the simulated *r*-values, namely r_{RD}, r_{45} and r_{TD}, of all the ideal texture components subject to UT-RD, UT-45^o and UT-TD respectively. Note that UT-45^o corresponds to a UT in the direction, which makes an angle of 45^o to RD. It can be seen in Table I that different texture components can have different plastic response in terms of *r*-value under the same type of deformation mode. Specifically, Goss and CG texture components have very high r_{TD} values, whereas S and CH components have rather low r_{TD}.

Meso-mechanical "Moving Window" simulation

In the present study, the MTM-FHM software system [9] is used to simulate the *r*-value based on the crystallographic texture. The "Moving Window" ("MW" for short hereafter) method is proposed to automate the *r*-value simulation with regard to the grain clusters. This "MW" is developed based on the test box method in Ref. [11], where the test box extends over the whole dimension along RD and moves only in TD. However, the "MW" can vary its size and move in both TD and RD. Note that a comparable band approach with a narrow band width has already been described in Refs. [8] and [12] and a static window approach in Ref. [13].

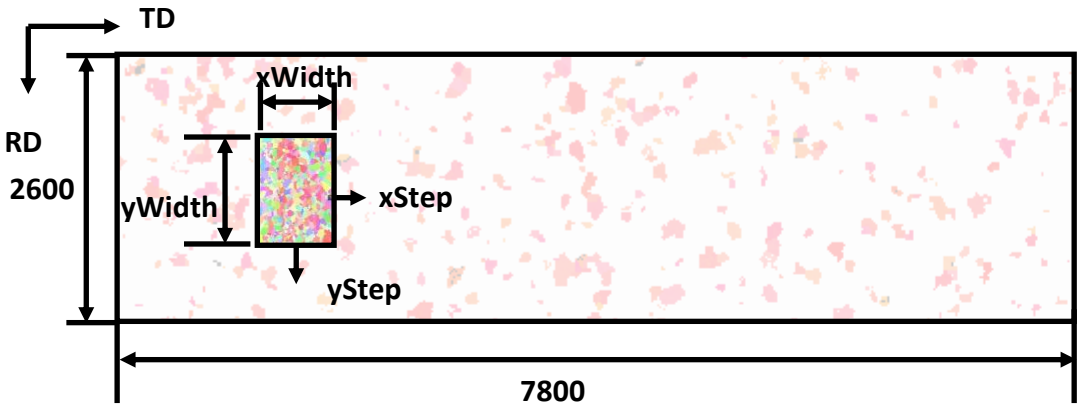

Fig. 2 Schematic illustration of the "MW" technique; The window with xWidth as the width in TD and yWidth as the width in RD can move either in TD at a step size of xStep or in RD at a step size of yStep.

By using a "MW" on top of the EBSD orientation map, a part of the grains can be selected as illustrated in Fig. 2. When the window size matches the characteristic dimension of the grain clusters, the characteristic local texture information can be extracted from the global EBSD texture data. Therefore, the local texture variation can be translated to *r*-value variation. Since *r*-value indicates strain thinning in ND, patterning in *r*-value could correlate to patterning of roping. Consequently, the roping tendency will be evaluated based on the "MW" technique in terms of *r*-value patterning.

Two window sizes, namely, 500 (μm) by 500 (μm) and 500 (μm) by 2600 (μm) (TD by RD), are adopted arbitrarily in this study. Specifically, the 500 by 500 window includes approximately 300 grains, while the 500 by 2600 window contains about 1500 grains. *r*-value variation along both TD and RD is simulated for UT-TD.

A step size of 16 μm is used for the present study, since the scanning step size of both EBSD measurements is 8 μm and the average grain size of both samples is approximately 30 μm. Thus, such a window step is fine enough to cover all the possible grains in both samples.

By making the window as large as the entire EBSD orientation maps for the two samples, the average *r*-values in different directions can be simulated based on the global EBSD texture. Table II shows the simulated *r*-values in *RD*, *45*^{o} and *TD* directions for both samples. Due to the presence of global textures in both samples, *r*-value varies under different UT directions. It can be obtained in Table II that UT-TD produces highest *r*-value for the roping susceptible sample, whereas UT-RD results in the highest *r*-value for the roping resistant sample. Both samples show lowest *r*-values under UT-45^{o}. It can be seen in Table II that the most strain thinning resistant direction for the EBSD measured layer/plane is TD for the roping susceptible sample, whereas it is RD for the roping resistant one.

Table II Simulated *r*-values in 3 UT-directions for the roping susceptible and resistant samples

Sample	r_{RD}	r_{45}	r_{TD}
Roping susceptible	0.77	0.21	0.95
Roping resistant	0.87	0.30	0.50

Results and discussions

Texture analysis by ODF shows that the roping susceptible sample has a stronger global texture than the roping resistant one. Besides, the volume fraction calculation of the typical texture components shows that the global texture constitution is quite similar for both samples except that the Goss texture component of the roping susceptible sample is more than twice as strong as the roping resistant one as shown in Table I. Furthermore, r_{TD} simulation distinguishes between the Goss or CG and the S or CH texture components with regard to the strain thinning resistance. It can be seen in Table I that the Goss or CG component has very high r_{TD} compared to random texture, while the S or CH component shows quite low r_{TD}. Therefore, Goss or CG component is expected to form peaks on the surface for UT-TD, whereas S or CH component is speculated to form valleys. It is worth noting that Goss component exhibits infinity for r_{TD}, making itself the most resistant texture component under UT-TD. Thus, even a small amount of Goss component may play a significant role in UT-TD mode. On the other hand, Goss component shows a low r_{45}.

In the literature [7, 14], the banding of texture components has been observed in AA6xxx alloys suffering from roping. Thus, the EBSD maps containing only Goss and CG grains within 16.5° misorientation are shown in Fig. 3 (a) and Fig. 3 (b) for the roping susceptible and resistant sample respectively. Fig. 3 (e) and Fig. 3 (f) show the EBSD maps with only grains within 16.5° misorientation of exact S and CH components for the roping susceptible and resistant sample respectively. It could be seen in both Fig. 3 (a) and Fig. 3 (b) that the Goss and CG grains are not distributed homogeneously but tend to form grain clusters. A similar observation could be made for S and CH maps in both roping susceptible and resistant samples as shown in Fig. 3 (e) and Fig. 3 (f). As the r_{TD} simulation based on the ideal model texture components suggests, Goss/CG orientation maps may serve to identify the peak positions on the UT-TD deformed sheet surface. Similarly, S/CH maps may be used to find the positions corresponding to the valleys on the sheet surface in UT-TD. However, this type of image analysis is quite subjective.

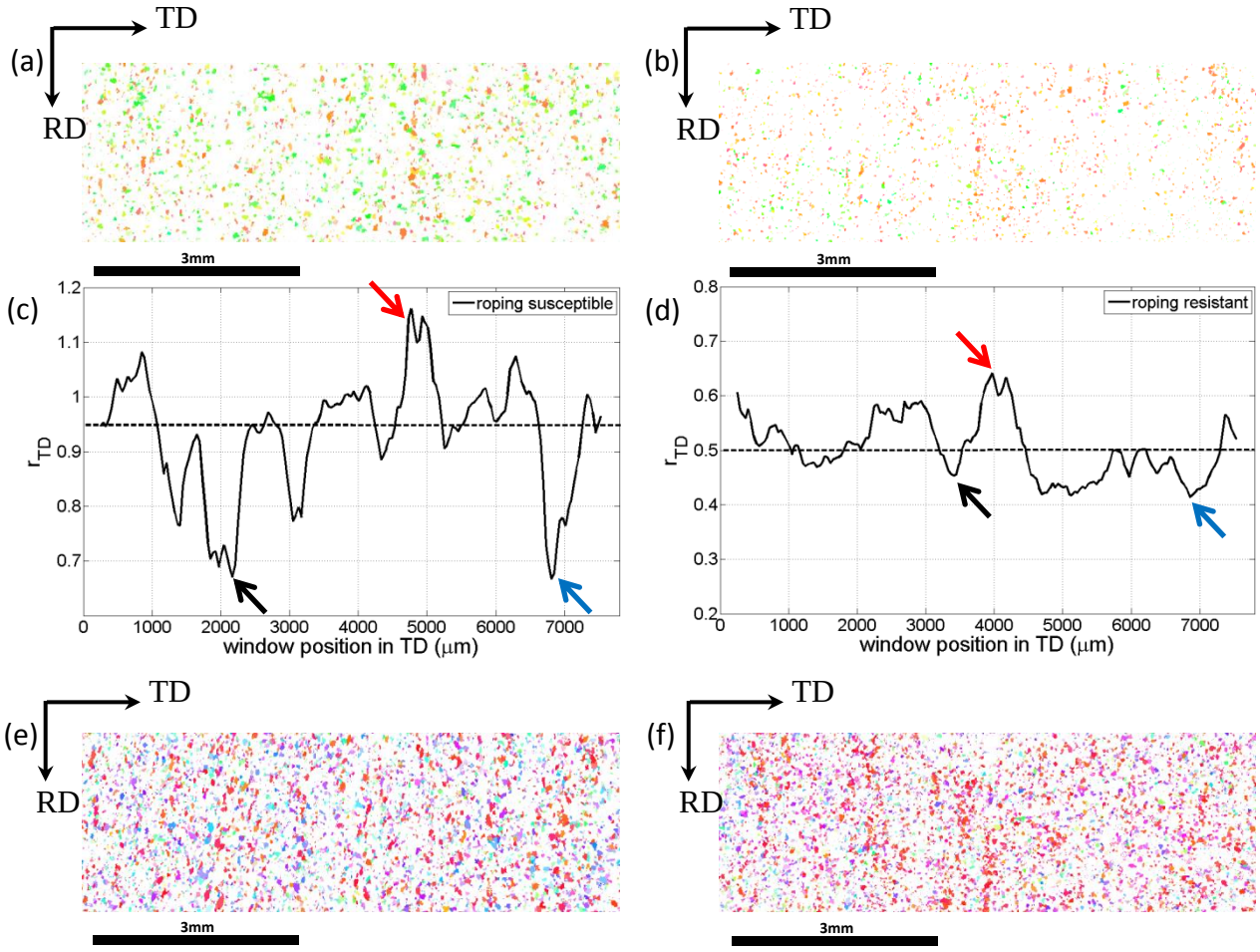

Fig. 3 EBSD orientation maps with only grains within 16.5° of exact Goss and CG components (a) for the roping susceptible sample and (b) for the roping resistant sample; simulated $\boldsymbol{r_{TD}}$ of a 500 by 2600 moving window vs. the window position from the left edge of the EBSD map in TD for the (c) roping susceptible and (d) resistant samples; (e) and (f) corresponding EBSD maps with only grains within 16.5° of exact S and CH components for the roping susceptible and resistant samples respectively. Note that the EBSD maps and the simulated $\boldsymbol{r_{TD}}$ figures are aligned with each other along TD for each sample.

The UT-TD simulation using a 500 by 2600 window moving at a step size of 16 μm along TD on the EBSD orientation map gives r_{TD} variation for both samples as shown in Fig. 3 (c) and (d). Note that the coordinate of a window center is used to represent its position. The extent of the vertical axis for r_{TD} is set the same for Fig. 3 (c) and (d), whereas the scales are different since the two samples have different average global r_{TD} values. The dashed lines in Fig. 3 (c) and (d) corresponding to the average global r_{TD} values of the roping susceptible and resistant samples lie at 0.95 and 0.5 respectively. The average *r*-values are shown in Table II. Thus the characterized layer of the roping susceptible sample is globally more resistant to strain thinning under UT-TD than that of the roping resistant sample.

By comparing Fig. 3 (c) with (d), it is seen that the roping susceptible sample shows a larger r_{TD} undulation than the roping resistant one. The r_{TD} difference between the highest peak and lowest valley is 0.5 and 0.23 for the roping susceptible and resistant samples respectively. Moreover, the roping susceptible sample shows evident r_{TD} waviness as indicated in Fig. 3 (c), whereas very moderate r_{TD} variation can be observed in the roping resistant sample as shown in Fig. 3 (d).

When a 500 by 500 window is used, the window position in both TD and RD should be defined. If the "MW" scans along TD, the window position, which is represented by its center coordinate, is given by the abscissa in an *r*-value vs. window position figure. Meanwhile, the window position in RD is given in the legend. Similarly, when the window moves in RD, its position in TD is shown in legend. Note that the x-coordinate increases from left to right, while y-coordinate increases from top to bottom in the EBSD map as illustrated in Fig. 2.

Fig. 4 shows the simulated r_{TD} for a 500 by 500 moving window vs. the window position along TD for both samples at 3 positions in RD. The 3 different scans along TD are made at positions 250 μm, 1250 μm and 2250 μm in RD. It can be seen in Fig. 4 that the roping susceptible sample shows much larger r_{TD} undulation along TD than the roping resistant one at all positions in RD except for the window position at 1250 μm in RD. In-phase correlation of r_{TD} curves at all window positions in RD can be observed in the roping susceptible sample as shown in Fig. 4 (a). However, there is no in-phase correlation for the roping resistant sample [see Fig. 4 (b)].

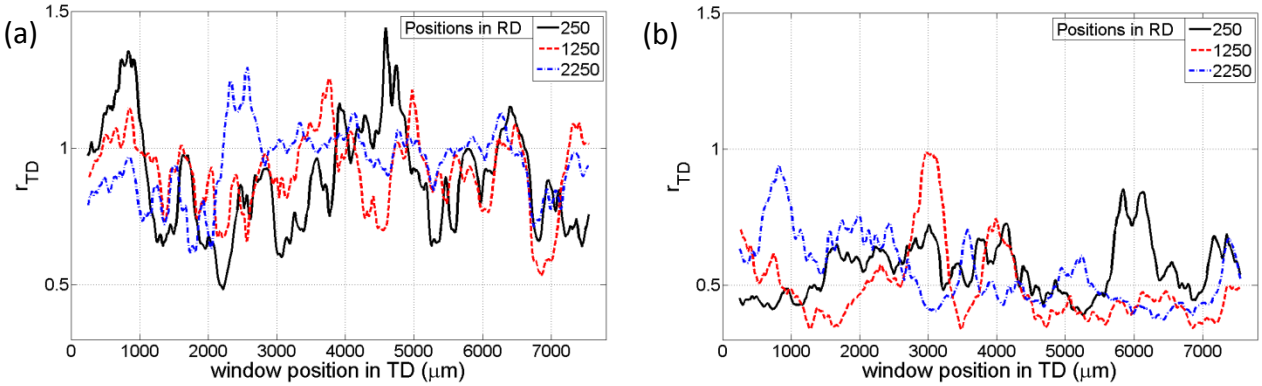

Fig. 4 simulated $\boldsymbol{r_{TD}}$ of a 500 by 500 moving window vs. the window position from the left edge of the EBSD map in TD for the (a) roping susceptible and (b) resistant samples, at different position in RD (increasing from top to bottom)

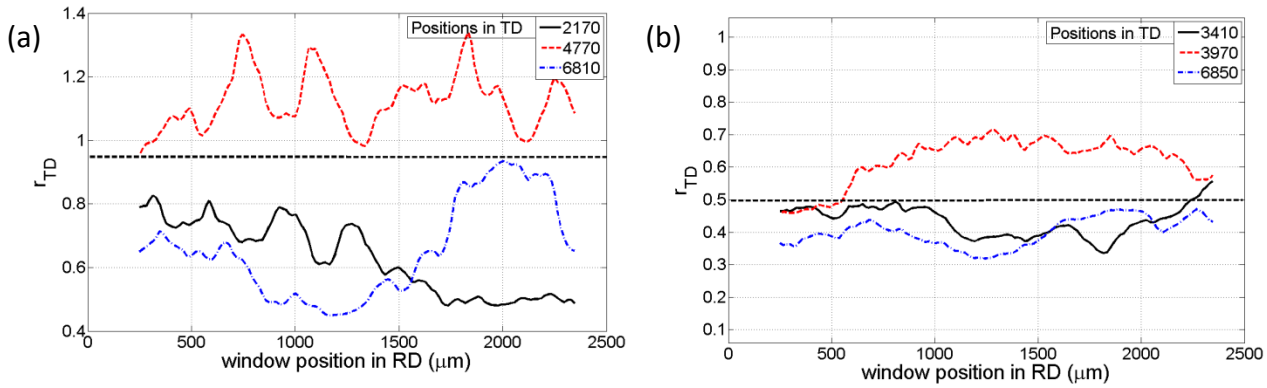

Fig. 5 simulated r_{TD} of a 500 by 500 moving window vs. the window position from the top edge of the EBSD map in RD for the (a) roping susceptible and (b) resistant samples, at different position in TD (increasing from left to right)

Fig. 5 shows the simulated r_{TD} variation for a 500 by 500 moving window when the "MW" scans from the top edge of the EBSD map to the bottom along RD at 3 positions in TD. These 3 window positions in TD (see Fig. 5) are corresponding to 1 peak and 2 valleys for both samples as shown in Fig. 3 (c) and (d). It can be seen for the roping susceptible sample in Fig. 5 (a) that r_{TD} for a 500 by 500 moving window at 4770 μm in TD is always higher than the average global r_{TD} value, while r_{TD} at 2170 μm and 6810 μm in TD is lower than the average r_{TD} value. This large r_{TD} distinction between the peak and valleys provides evidence for the formation of continuous peak and valleys. Fig. 5 (b) also shows the separation of r_{TD} between a peak and two valleys in the roping resistant sample. However, the simulated r_{TD} based on 500 by 500 "MW" is very close to the average r_{TD} value. Consequently, comparing Fig. 3 (c) and (d) with Fig. 5 can explain why peaks and valleys form along TD in the roping susceptible sample but not in the roping resistant sample.

Although it is indicated that the valleys marked by arrows are the highly possible locations suffering from strain thinning as shown in Fig. 3 (c), it is not so convincing to correlate these locations with S/CH bands. Only a weak correlation can be built between Goss/CG deficient regions and valleys by comparing Fig. 3 (a) and Fig. 3 (c).

It can also be seen in Fig. 5 (a) that minor r_{TD} undulation occurs in RD. This undulation suggests that minor surface roughening in RD should result. This is in agreement with the experimental observation as shown in Fig. 5(b) in Ref. [8]. So far, all the r_{TD} simulations [see Fig. 3 (c) and (d), Fig. 4 and Fig. 5] suggest a higher surface roping propensity for the roping susceptible sample than the roping resistant one. . Therefore, the r_{TD} simulation based on the "MW" method is capable of predicting the roping behavior of AA6016 aluminium alloys subject to UT-TD.

Conclusions

The "Moving Window" method provides the direct evidence of the possibility of depression coalescence to form continuous grooves characteristic of roping material. Besides, the "Moving Window" method has been shown to be able to identify roping tendency qualitatively.

Future work

The "Moving Window" method can be extended to analyze the roping or ridging phenomenon quantitatively, if an optimized window size can be obtained based on the characteristic of the experimental roping profile and microstructure. By assuming a proper homogeneous volume corresponding to the optimal "Moving window", one can compute "valleys" and "ridges", which will correspond to the surface of the "Moving window". Then, a quantitative criterion can be built for the roping analysis. This will be published later in a journal.

Acknowledgement

The authors gratefully acknowledge the financial support provided by IAP-7/21 project. L. Qin would also like to thank P. Eyckens, Q. Xie and X. Wang (MTM, KU Leuven) for their patient explanation and fruitful discussion.

Reference

1. Hirsch, J., *Aluminium in Innovative Light-Weight Car Design.* Materials Transactions, 2011. **52**(5): p. 818-824.

2. Engler, O. and J. Hirsch, *Texture control by thermomechanical processing of AA6xxx Al-Mg-Si sheet alloys for automotive applications - a review.* Materials Science and Engineering a-Structural Materials Properties Microstructure and Processing, 2002. **336**(1-2): p. 249-262.

3. Wu, P.D., et al., *Analysis of roping in AA6111 automotive sheet.* Acta Materialia, 2003. **51**(7): p. 1945-1957.

4. Baczynski, G.J., et al., *Development of roping in an aluminum automotive alloy AA6111.* Acta Materialia, 2000. **48**(13): p. 3361-3376.

5. Beaudoin, A.J., J.D. Bryant, and D.A. Korzekwa, *Analysis of ridging in aluminum auto body sheet metal.* Metallurgical and Materials Transactions a-Physical Metallurgy and Materials Science, 1998. **29**(9): p. 2323-2332.

6. Raabe, D., et al., *Grain-scale micromechanics of polycrystal surfaces during plastic straining.* Acta Materialia, 2003. **51**(6): p. 1539-1560.

7. Bennett, T.A., R.H. Petrov, and L.A.I. Kestens, *Texture-induced surface roping in an automotive aluminium sheet.* Scripta Materialia, 2009. **61**(7): p. 733-736.

8. Engler, O., C. Schäfer, and H.J. Brinkman, *Crystal-plasticity simulation of the correlation of microtexture and roping in AA 6xxx Al–Mg–Si sheet alloys for automotive applications.* Acta Materialia, 2012. **60**(13-14): p. 5217-5232.

9. Van Houtte, P., *The MTM-FHM Software System*, 2004: Katholieke Universiteit Leuven, Belgium.

10. Xie, Q., et al., *Polycrystal plasticity models based on crystallographic and morphologic texture: Evaluation of predictions of plastic anisotropy and deformation texture.* Materials Science and Engineering: A, 2013. **581**: p. 66-72.

11. Qin, L., et al., *Mesoscopic EBSD Analysis and Mesomechanical Behavior of Ridging or Roping in AA6XXX Alloys*, in *the 16th International Conference on Textures of Materials (ICOTOM 16)*, A. Tewari, et al., Editors. 2011: IIT Mumbai, India. p. 955-958.

12. Engler O., H.M.-Y., Tome C.N. , *Crystal-plasticity analysis of ridging in ferritic stainless steel sheets* Metallurgical and Materials Transactions A: Physical Metallurgy and Materials Science, 2005. **36**(11): p. 3127-3139.

13. Wittridge, N.J. and R.D. Knutsen, *A microtexture based analysis of the surface roughening behaviour of an aluminium alloy during tensile deformation.* Materials Science and Engineering: A, 1999. **269**(1-2): p. 205-216.

14. Jin, H., et al., *Three-dimensional texture determination of 6111 aluminium alloy sheet by precise serial sectioning and EBSD measurement.* Materials Science and Technology, 2005. **21**(4): p. 419-428.